ACADEMIC PRESS

Available online at www.sciencedirect.com
SCIENCE DIRECT®

Journal of Catalysis 215 (2003) 7–13

JOURNAL OF CATALYSIS

www.elsevier.com/locate/jcat

# MAS NMR, TPR, and TEM studies of the interaction of NiMo with alumina and silica–alumina supports

Lianglong Qu,[a] Weiping Zhang,[a] Patricia J. Kooyman,[b] and Roel Prins [a,*]

[a] *Laboratory for Technical Chemistry, Federal Institute of Technology, ETH-Hönggerberg, 8093 Zurich, Switzerland*
[b] *National Centre for HREM, Delft University of Technology, Rotterdamseweg 137, 2628 AL Delft, The Netherlands*

Received 21 June 2002; revised 24 October 2002; accepted 25 November 2002

**Abstract**

$^{1}$H MAS NMR, $^{1}$H spin-echo MAS NMR with Al irradiation, $^{29}$Si MAS NMR, and $^{1}$H → $^{29}$Si CP MAS NMR were used to investigate the deposition of Mo and Ni species on the surface of alumina and silica–alumina. Mo and Ni species first occupy the alumina sites and then the silica sites. The results of temperature-programmed reduction show that the weaker interaction between the Mo and Ni species and the silica–alumina support leads to better reducibility of the metal oxides on silica–alumina than on $Al_2O_3$. Mo and Ni species also interact with each other. Transmission electron microscopy proved that, after sulfidation, higher stacks of $MoS_2$ are formed on the silica–alumina support than on the $Al_2O_3$ support. The higher stacking is responsible for the higher hydrodenitrogenation activity of the NiMoS catalysts supported on silica–alumina.


*Keywords:* NMR; TPR; TEM; Interaction; Support; NiMo; Hydrotreating; Alumina; Silica–alumina

## 1. Introduction

Supported nickel–molybdenum catalysts are extensively used in hydrotreating, one of the most important processes in oil refining [1]. These catalysts are usually prepared by depositing molybdenum and nickel oxides on the surface of oxidic supports such as alumina ($Al_2O_3$) and silica–alumina ($SiO_2$–$Al_2O_3$). The catalysts are used in the active, sulfided state, and the nature and properties of the oxide precursors largely determine the performance of the catalysts. Many studies focused on the nature and structure of the Mo species, and the results of studies employing many characterization techniques indicate that the presence of the promoter atoms does not greatly affect the state of the Mo species on the $Al_2O_3$ surface. Since $Al_2O_3$ is the most commonly used support, most studies have focused on Mo oxides supported on $Al_2O_3$ (see, e.g., [2–7]). Several studies dealt with $SiO_2$-supported Mo [8–15], whereas few studies dealt with $SiO_2$–$Al_2O_3$-supported systems [8,9,12,16–18]. It is generally accepted that Mo oxide on an $Al_2O_3$ support forms amorphous monolayers or "islands" on the $Al_2O_3$ at an Mo loading below 5 atoms/nm$^2$ owing to the strong interaction with the support [19,20]. The Mo species was identified as octahedrally or tetrahedrally coordinated [21,22]. On $SiO_2$ supports, the same octahedrally and tetrahedrally coordinated species are formed, in addition to bulk, orthorhombic $MoO_3$, even at very low Mo loadings [21,23]. However, less agreement was reached with respect to the silica–alumina-supported catalysts.

Solid-state NMR was used to characterize hydrotreating catalysts [4,7,24–31]. Most studies concentrated on the Mo structure and the effect of additives by measuring the $^{27}$Al, $^{95}$Mo, and $^{31}$P NMR spectra. $^{1}$H MAS NMR was used for the structural investigation of hydroxyl groups on $Al_2O_3$-supported Mo catalysts [4,7,26]. However, $^{29}$Si NMR was not used in hydrotreating catalysis, although one example was reported in a recent patent [32].

In previous studies [33,34], we reported that the performance of NiMo catalysts supported on amorphous silica–alumina (ASA) is outstanding in hydrodenitrogenation but that a higher hydrogenation activity was found on $Al_2O_3$-supported catalysts. In the present study, we tried to understand the interaction of the Mo and Ni species with the support. Much attention was paid to the ASA-supported catalysts, and $Al_2O_3$-supported catalysts were studied for com-

* Corresponding author.
*E-mail address:* prins@tech.chem.ethz.ch (R. Prins).

0021-9517/03/$ – see front matter 
doi:10.1016/S0021-9517(02)00181-1

parison. $^1$H MAS NMR and $^1$H spin-echo MAS NMR with Al irradiation were used to identify and monitor changes in the surface OH groups. $^{29}$Si MAS NMR and $^1\text{H} \rightarrow {}^{29}\text{Si}$ CP MAS NMR were used to characterize the evolution of the surface Si sites and, in turn, the Al sites. TPR was used to elucidate the phases of Mo and Ni species in the catalysts and TEM to study the $MoS_2$ stacking of the sulfided catalysts.

## 2. Experimental

### 2.1. Catalyst preparation

NiMo catalysts supported on alumina (Condea) and silica–alumina (Shell, containing 75 wt% $SiO_2$, prepared with the sol–gel method) were prepared by successive pore volume impregnation (Mo first) with aqueous solutions containing the appropriate amounts of ammonium molybdate tetrahydrate (Fluka) and nickel nitrate hexahydrate (Fluka). The impregnated materials were dried overnight in air at 120 °C and further calcined at 500 °C for 4 h after each impregnation step (heating rate 3 °C/min). The final catalysts contained 2.9 wt% Ni and 8.8 wt% Mo, as analyzed by AAS. The $Al_2O_3$-supported catalyst had a surface area of 202 $m^2/g$ and a pore volume of 0.33 ml/g with a narrow pore size distribution, at around 5.6-nm diameter, as determined by BET $N_2$ adsorption. The ASA-supported catalyst had a surface area of 296 $m^2/g$ and a pore volume of 0.44 ml/g with a narrow pore size distribution at around 5.3 nm.

### 2.2. MAS NMR measurements

All the NMR spectra were obtained at 9.4 T on a Bruker AMX-400 spectrometer. $^{29}$Si MAS NMR spectra were recorded at 79.5 MHz using a 2-μs ($\pi/4$) pulse with a 4-s recycle delay and 6000 scans. $^1\text{H} \rightarrow {}^{29}\text{Si}$ CP/MAS NMR experiments were performed with a 4-s recycle delay, 8000 scans, and a contact time of 10 ms. All the $^{29}$Si spectra were collected using 7-mm $ZrO_2$ rotors at a spinning rate of 5 kHz; chemical shifts were referenced to $Q_8M_8$ (cubic octamer silicic acid trimethylsilyl ester). Before the $^1$H MAS NMR measurements, samples were dehydrated at 400 °C and at a pressure below $10^{-2}$ Pa for 15 h. $^1$H MAS NMR spectra were recorded at 400.2 MHz by a spin-echo pulse sequence ($\frac{\pi}{2}$–$\tau$–$\pi$–$\tau$–acquire), where $\tau$ was set to one rotor period and the excitation pulse length was 4.5 μs ($\frac{\pi}{2}$). $^1\text{H}\{^{27}\text{Al}\}$ spin-echo double-resonance experiments were performed according to the method of van Eck et al. [35]. In this experiment, a spin-echo pulse was applied to the $^1$H channel and aluminum was irradiated simultaneously during the first $\tau$ period. The $^{27}$Al irradiation field was about 60 kHz. All the $^1$H spectra were accumulated for 128 scans with a 10-s recycle delay and using 4-mm $ZrO_2$ rotors spun at 10 kHz. The chemical shifts were referenced to adamantane ($\delta = 1.74$ ppm). The modified Winfit software Dmfit 98 was employed for deconvolution using Gaussian lineshapes. The fitting errors for our spectra were estimated to be about 7%.

### 2.3. Temperature-programmed reduction (TPR)

TPR measurements were conducted with a Micromeritics AutoChem 2910 Automated Catalyst Characterization System. About 0.2 g of sample was used for each measurement. A mixture of 4.8 vol% $H_2$/Ar was introduced at 50 ml/min into the sample loop and was also used as a reference gas. The sample was heated at a rate of 10 °C /min to 900 °C and was maintained at this temperature for 30 min. The effluent gas was passed through a viscous solution of isopropanol, cooled by liquid $N_2$ to remove the water produced during reduction, and analyzed with a thermal conductive detector.

### 2.4. Transmission electron microscopy (TEM)

The catalysts were sulfided quasi in situ in a mixture of 10 vol% $H_2S/H_2$. The gas flow was kept at 150 ml/min, whereas the catalyst was heated at a rate of 6 °C/min to 370 °C. The temperature was then kept at 370 °C for 4 h. Subsequently, the sample was cooled to room temperature under flowing high-purity $N_2$. Then the sample was sealed in the reactor and transferred to a glovebox.

TEM measurements were performed using a Philips CM30T electron microscope with an $LaB_6$ filament as the source of electrons operated at 300 kV. Samples were mounted on a microgrid carbon polymer supported on a copper grid by placing a few droplets of a suspension of the ground sample in *n*-hexane on the grid, followed by drying under ambient conditions, all in an Ar glovebox. The samples were transferred to the microscope in a special vacuum-transfer sample holder under exclusion of air [36].

At least 10 representative micrographs were taken for each catalyst in high-resolution mode. Typically, the length ($L$) and number of the stacks ($n$) of at least 250 slabs were measured for each catalyst.

## 3. Results and discussion

### 3.1. MAS NMR

High-resolution $^1$H MAS NMR is a useful and straightforward tool for characterizing the hydroxyl groups in alumina and zeolites. It can provide quantitative information about the interaction between metal ions and hydroxyl groups on the support without the difficulties associated with extinction coefficients that are encountered in IR spectroscopy. Fig. 1a illustrates the $^1$H MAS NMR spectra obtained for the $\gamma$-$Al_2O_3$ support and the $NiMo/Al_2O_3$ catalyst. As expected, there were two main peaks. The peak at 1.9 ppm is attributed to the acidic hydroxyl groups on

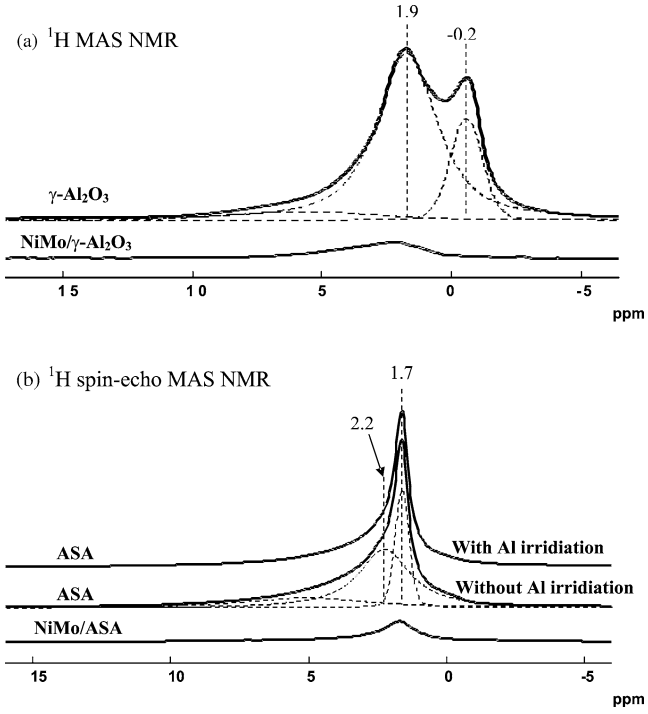


Fig. 1. $^1$H MAS NMR spectra of supports and catalysts. (a) $Al_2O_3$ support and NiMo/$Al_2O_3$; (b) ASA support and NiMo/ASA.

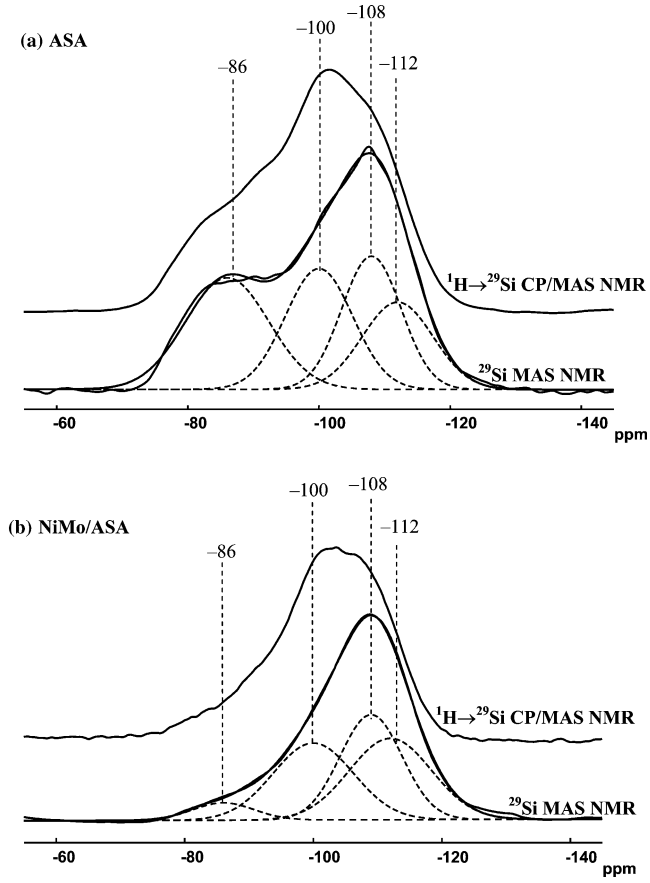


Fig. 2. $^{29}$Si MAS NMR and $^1$H → $^{29}$Si CP/MAS NMR spectra of (a) ASA support and (b) NiMo/ASA catalyst.

the alumina surface and the other at −0.2 ppm to the basic hydroxyl groups [7,37,38]. With quantitative deconvolution of the spectrum, a broad shoulder at around 5.2 ppm can also be identified. It is ascribed to a small amount of physisorbed and chemisorbed water on the alumina or silica–alumina surface [38]. After impregnation with Mo and Ni, the total number of hydroxyl groups on the alumina surface decreased substantially, and the basic hydroxyls at −0.2 ppm were preferentially reduced compared to the acidic hydroxyls at 1.9 ppm. It is agreed that Mo species adsorb preferentially on the basic hydroxyl groups on $Al_2O_3$ support [7,39]. The preferential disappearance of the basic hydroxyl groups at −0.2 ppm might also be due to the paramagnetic Ni in the vicinity of hydroxyl groups. When we compare the results obtained here with those from only Mo supported on $Al_2O_3$ [7,39], however, this possibility can be excluded. The basic hydroxyls are preferentially occupied, also upon deposition of F and P on $Al_2O_3$ [4,24].

In the case of ASA, an asymmetric signal was found in the NMR spectrum (Fig. 1b). After deconvolution, three lines were obtained. As indicated above, the broad line at about 5.0 ppm can be assigned to a trace amount of physisorbed and chemisorbed water on ASA [38]. The peak at 1.7 ppm may be tentatively ascribed to surface silanol groups, whereas the peak at about 2.2 ppm may be attributed to OH groups attached to aluminium species or to another kind of hydrogen-bonded silanol group [40]. To clarify this, $^1$H{$^{27}$Al} spin-echo double-resonance experiments were carried out, which is analogous to the dipolar dephasing experiment described by Fyfe et al. [41]. Under strong aluminium irradiation during the spin-echo pulse sequence applied to the proton, the signal of the proton groups that are strongly coupled to aluminium will be significantly suppressed, whereas the other protons will be unaffected. Therefore, it offers the possibility of differentiating between the OH signals of species close to an aluminium atom and those of species which are farther away. As shown in the spectra of the ASA support (Fig. 1b), the intensity of the peak at 2.2 ppm decreases with Al irradiation, whereas the peak at 1.7 ppm remains unchanged. Thus, we deduced that the peak at 2.2 ppm is the result of the hydroxyl protons associated with aluminium species and that at 1.7 ppm should be assigned to the silanol protons.

A quantitative analysis showed that the ratio of the surface aluminium hydroxyl groups (AlOH) to silanol groups (SiOH) is 2.2 on the ASA support, whereas this ratio decreased to 0.5 for the NiMo/ASA catalyst. The surface AlOH groups decreased in intensity by 94% after impregnation with Mo and Ni species, whereas the SiOH groups decreased by 72%. This indicates that Ni and Mo species adsorb preferentially on the AlOH sites on the ASA support.

The ASA support and the NiMo/ASA catalyst were further studied using $^{29}$Si MAS NMR and $^1$H → $^{29}$Si CP/MAS NMR (Figs. 2a and 2b). After careful deconvolution of the $^{29}$Si MAS NMR spectra, four peaks were obtained quantita-

tively. The peaks at −112 and −108 ppm are ascribed to the $Si(OSi)_4$ and $Si(OSi)_3(OAl)$ groups, respectively [42–44]. The peaks at −100 and −86 ppm are ascribed to terminal silanol groups as in $Si(OH)(OSi)_3$ and $Si(OH)_2(OSi)_2$, respectively [45,46]. The assignment of the silanol groups is facilitated by the use of the $^1H \rightarrow {}^{29}Si$ cross-polarization technique [45,47]. As demonstrated in Fig. 2, application of the CP technique selectively enhances the signals at −100 and −86 ppm of silicon atoms, which are coupled with protons of hydroxyl groups by dipolar $^1H$–$^{29}Si$ interaction. In comparing the spectra of the ASA support with the ASA-supported catalyst, a strong decrease in intensity was observed at −86 ppm and a slight decrease at −100 ppm. This indicates that Mo and Ni species interact with the silanol groups and are adsorbed more easily on the geminal silanols.

### 3.2. TPR

The interactions between Mo and the supports were further studied by TPR. To evaluate the interaction between Ni and Mo species, catalysts containing only Ni or Mo were measured as well (Figs. 3 and 4). Under the applied conditions, all the species can be reduced. For $Ni/Al_2O_3$ (Fig. 3), the maximum reduction temperature is shown as a broad band centered between 640 and 800 °C, which is a higher temperature than for bulk NiO, which shows a single reduction peak at around 300 °C [8]. For $Mo/Al_2O_3$, two main peaks, one at 422 °C and the other at 874 °C, and a shoulder were observed at 710 °C. The low-temperature peak can be assigned to the partial reduction ($Mo^{6+} \rightarrow Mo^{4+}$) of amorphous, highly defective, multilayered Mo oxides or

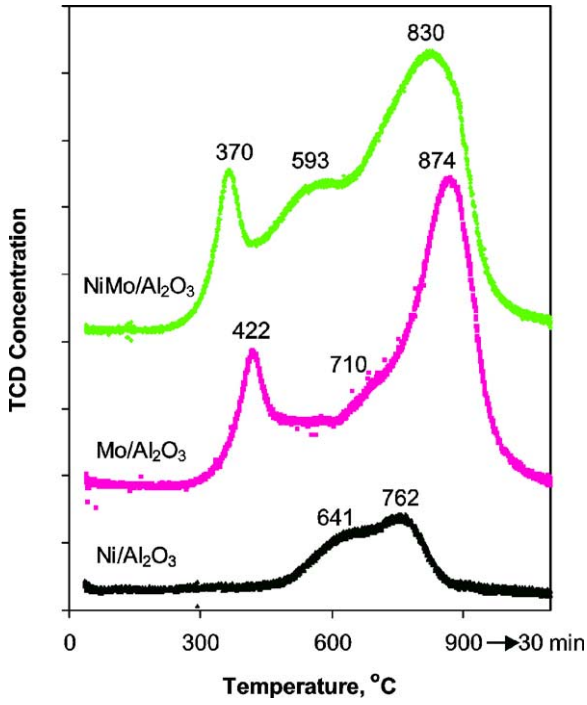


Fig. 3. TPR patterns of Ni, Mo, and NiMo supported on $Al_2O_3$.

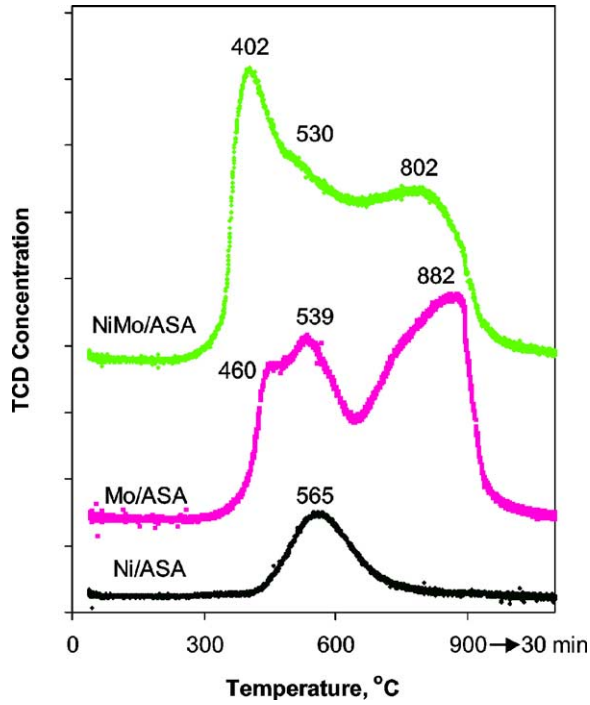


Fig. 4. TPR patterns of Ni, Mo, and NiMo supported on ASA.

heteropolymolybdates (octahedral Mo species) [12,21,48]. The high-temperature peak at 874 °C comprises the deep reduction of all Mo species, including highly dispersed tetrahedral Mo species. The peak at 710 °C may be due to the intermediate-reducible crystalline phases of orthorhombic $MoO_3$ and $Al_2(MoO_4)_3$ [18,48–50]. After incorporation of Ni into $Mo/Al_2O_3$, the TPR profile shifted to lower temperature (cf. $NiMo/Al_2O_3$ in Fig. 3). Peaks were observed at 370, 593, and 830 °C. When the Ni content and calcination temperature of the NiMo catalysts were changed, the peak at 593 °C was assigned to the reduction of Ni species [8]. Both peaks for the Mo species shifted by 40 to 50 °C to a lower temperature, indicating that the addition of Ni promoted the reducibility of Mo. At the same time, the reduction of the Ni species was promoted from 640 to 800 °C for the reduction of $Ni/Al_2O_3$ to 593 °C for the reduction of the Ni species in $NiMo/Al_2O_3$. This suggests that there was an interaction between Ni and Mo species.

For Ni/ASA (Fig. 4) the peak reduction temperature is 565 °C, which is lower than that for $Ni/Al_2O_3$, indicating a weaker interaction between Ni and the ASA support. The TPR spectrum for Mo/ASA shows two regions, a broad band with peaks at 460 and 539 °C and another band at 882 °C. Compared with the spectrum of $Mo/Al_2O_3$ (Fig. 3), there are more easily reducible species in the Mo/ASA sample, suggesting that the interaction between the Mo species and the ASA support is weaker than that between the Mo species and the $Al_2O_3$ support. After the addition of Ni to the Mo/ASA, the reduction peaks of the Mo species shifted to 402 and 802 °C (cf. NiMo/ASA in Fig. 4). The major part of the Mo species was reduced at a lower

temperature. The reduction of Ni species was also promoted, showing a maximum at 530 °C.

A comparison of the TPR spectra of the NiMo catalysts supported on $Al_2O_3$ and ASA (Figs. 3 and 4) showed that there are more easily reducible Mo species in the ASA-supported catalyst than in the $Al_2O_3$-supported catalyst. The reduction peaks for both the Ni and Mo species shifted to lower temperature. This is in agreement with the results of Rajagopal et al. [18], who studied Mo catalysts supported on a series of silica–alumina of different composition. They found that the extent of reduction increases with $SiO_2$ content, reaching a maximum at the composition $SiO_2$:$Al_2O_3$ = 75:25 (wt%) for a fixed Mo loading. A relationship between reducibility and catalytic activity was established for Mo-containing catalysts [19,51,52]; this may, to some extent, explain the difference in activity caused by the different supports. The lower hydrogenation activity for cyclohexene over the NiMo/ASA catalyst [33] may be related to the higher reduction temperature (402 °C, the first peak for NiMo/ASA in Fig. 4) compared to the reduction temperature for $NiMo/Al_2O_3$ (370 °C in Fig. 3). A relation between hydrodenitrogenation activity and reducibility has, however, not been reported.

We also checked for Mo oxide species by XRD, but no crystalline phases of Mo, Ni, or $Al_2(MoO_4)_3$ were detected in the $Al_2O_3$- and ASA-supported catalysts. They are all amorphous, suggesting that even though the interaction of Mo and Ni with ASA is weaker than with $Al_2O_3$, it is not weak enough to form crystalline phases. We can not rule out the formation of less crystalline $MoO_3$, or $Al_2(MoO_4)_3$, which can not be detected by XRD. This differs from the results of Massoth et al. [16] and Rajagopal et al. [18]. They found proof of three-dimensional Mo species in catalysts with supports containing 75 wt% or more of $SiO_2$ in their silica–alumina samples. One reason may be that they used a higher calcination temperature (540 to 550 °C) and a longer calcination time for preparing their catalysts.

### 3.3. TEM

The TEM micrographs of the sulfided catalysts clearly show the edge planes of $MoS_2$-like slabs oriented in line with or slightly tilted from the electron beam. Fig. 5 shows a representative TEM micrograph of sulfided $NiMo/Al_2O_3$. The slabs are homogeneously distributed over the $Al_2O_3$ surface. The $MoS_2$-like structures are made up of small ordered sections, which are often bent on a longer scale, suggesting a strong interaction with the support surface. The number of stacking layers is between 1 and 2, with an average of 1.8 layers. The average slab length is calculated to be 48 Å. For NiMo/ASA (Fig. 6), the slabs tend not to be homogeneously distributed. Some nest like stacks, in which several slabs are cross-linked, were observed in some of the micrographs. The stacks are higher than those in the case of $Al_2O_3$ and can consist of up to 6 layers. The average number of stacking is 2.6 layers and the average slab length is the same as that in $NiMo/Al_2O_3$.

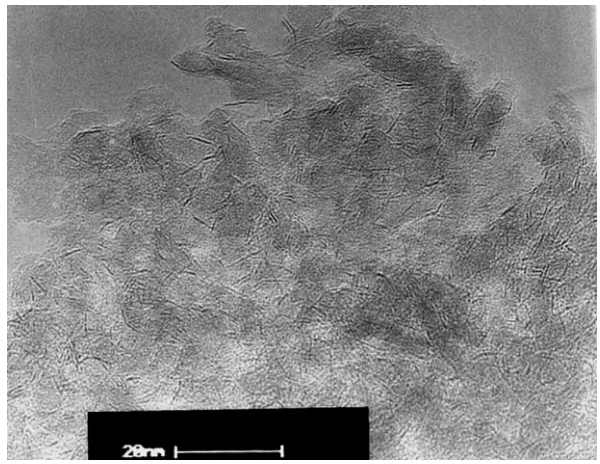

Fig. 5. TEM image of sulfided $NiMo/Al_2O_3$.

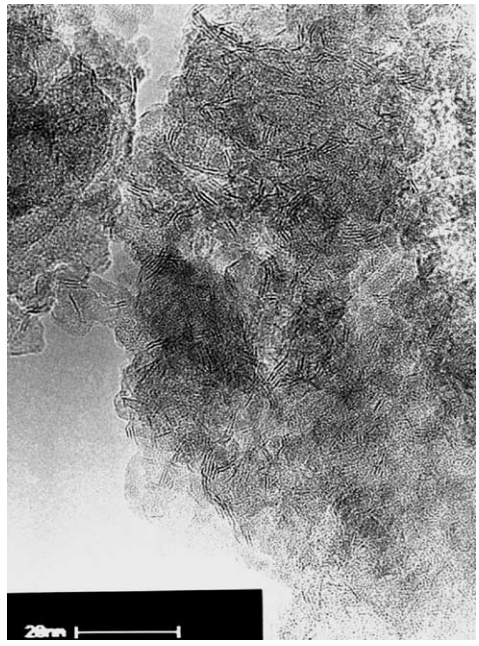

Fig. 6. TEM image of sulfided NiMo/ASA.

From the distribution of $MoS_2$ stacking (Fig. 7), higher stacking was observed for the ASA-supported catalyst than for its $Al_2O_3$-supported counterpart. About 35% of the distinguishable $MoS_2$ slabs in the $Al_2O_3$-supported catalyst are present as single layers, 50% as double layers, and 15% in three and four layers. For the ASA-supported catalyst, a relatively larger number of slabs present are stacked higher: fewer than 10% in single layers, 55% in double layers, 20% in three layers, and 15% in crystallites with between 4 and 6 layers. This confirms the weaker interaction between the ASA support and the Mo species. With higher stacking at the same slab length, there are more edge and corner sites on the ASA-supported catalysts than on the $Al_2O_3$-supported catalyst. Analogous to the “rim-edge”

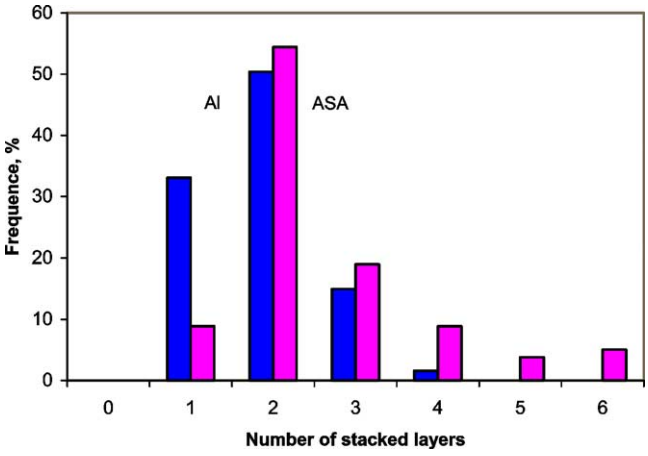


Fig. 7. Stacking distribution (black, $NiMo/Al_2O_3$; grey, NiMo/ASA).

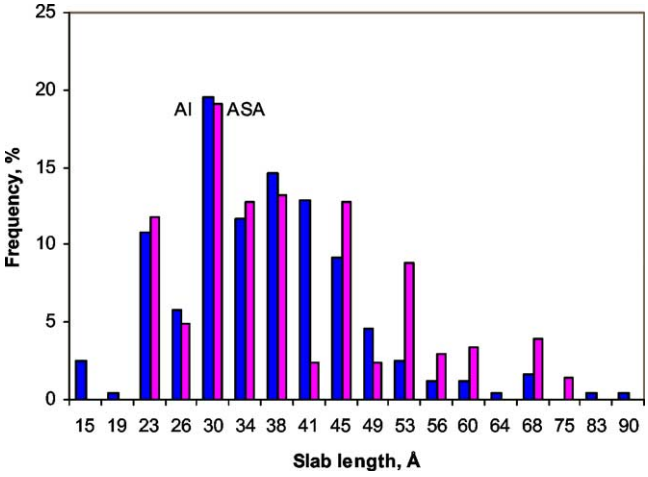


Fig. 8. Slab length distribution (black, $NiMo/Al_2O_3$; grey, NiMo/ASA).

model proposed by Daage and Chianelli for HDS [53], hydrodenitrogenation may occur on the corner and edge sites and hydrogenation of the phenyl ring only on the corner sites. The higher hydrodenitrogenation activity over the ASA-supported catalysts [34] suggests that the edge and corner sites are responsible for the hydrodenitrogenation reaction. The distribution of the slab lengths was broader for the ASA-supported catalyst than for its $Al_2O_3$-supported counterpart (Fig. 8), in line with the more heterogeneous distribution of the slabs in the ASA-supported catalyst.

## 4. Conclusions

MAS NMR was used to study the structure of oxidic NiMo catalysts supported on alumina and silica–alumina. Mo and Ni species on the ASA support preferentially adsorb on the alumina sites, but they can also be located on the silica sites after saturation of the alumina sites.

A weaker interaction of Mo and Ni species with the ASA support leads to a better reducibility of the Mo and Ni oxides than on the $Al_2O_3$ support. Interaction between Ni and Mo species also contributes to the reduction.

A lower dispersion of the Mo species in the oxidic state, due to the weaker interaction with the ASA support, is the cause of the higher stacking of $MoS_2$ in the sulfidic form. This in turn leads to a higher hydrodenitrogenation activity over the ASA-supported catalysts.

## References

[1] H. Topsøe, B.S. Clausen, F.E. Massoth, in: J.R. Anderson, M. Boudart (Eds.), Hydrotreating Catalysis Science and Technology, Springer, Berlin, 1996.
[2] F.E. Massoth, Adv. Catal. 27 (1978) 265.
[3] E. Payen, J. Grimblot, S. Kasztelan, J. Phys. Chem. 91 (1987) 6642.
[4] B.M. Reddy, V.M. Mastikhin, in: M.J. Phillips, M. Terman (Eds.), Proceedings 9th International Congress on Catalysis, Calgary (1988), Chemical Institute of Canada, Ottawa, 1988, p. 82.
[5] B. Scheffer, P. Arnoldy, J.A. Moulijn, J. Catal. 112 (1988) 516.
[6] N.-Y. Topsøe, H. Topsøe, J. Catal. 139 (1993) 631.
[7] C.J.H. Jacobsen, N.-Y. Topsøe, H. Topsøe, L. Kellberg, H.J. Jakobsen, J. Catal. 154 (1995) 65.
[8] J. Brito, J. Laine, Polyhedron 5 (1986) 179.
[9] R. Thomas, E.M. van Oers, V.H.J. de Beer, J.A. Moulijn, J. Catal. 84 (1983) 275.
[10] H. Shimada, T. Sato, Y. Yoshimura, J. Hiraishi, A. Nishijima, J. Catal. 110 (1988) 275.
[11] J.J.P. Biermann, F.J.J.G. Janssen, M. de Boer, A.J. van Dillen, J.W. Geus, E.T.C. Vogt, J. Mol. Catal. 60 (1990) 229.
[12] M. Henker, K.-P. Wendlandt, J. Valyon, P. Bornmann, Appl. Catal. 69 (1991) 205.
[13] H.M. Ismail, M.I. Zaki, G.C. Bond, R. Shukri, Appl. Catal. 72 (1991) L1.
[14] R. López Cordero, F.J. Gil-Llambías, A. López Agudo, Appl. Catal. 74 (1991) 125.
[15] T.-C. Liu, C.-S. Chang, J. Chin. Inst. Chem. Eng. 22 (1991) 285.
[16] F.E. Massoth, G. Muralidhar, J. Shabtai, J. Catal. 85 (1984) 53.
[17] M. Henker, K.-P. Wendlandt, E.S. Spiro, O.P. Tkachenko, Appl. Catal. 61 (1990) 353.
[18] S. Rajagopal, H.J. Marini, J.A. Marzari, R. Miranda, J. Catal. 147 (1994) 417.
[19] R. Thomas, E.M. van Oers, V.H.J. de Beer, J. Madema, J.A. Moulijn, J. Catal. 76 (1982) 241.
[20] Y. Okamoto, T. Imanaka, J. Phys. Chem. 92 (1988) 7102.
[21] R. Thomas, M.C. Mittelmeijer-Hazeleger, F.P.J.M. Kerkhof, J.A. Moulijn, J. Medema, V.H.J. de Beer, in: H.F. Barry, P.C.H. Mitchell (Eds.), Proceedings of the 3rd Climax International Conference on the Chemistry and Uses of Molybdenum, Climax Molybdenum, Ann Arbor, MI, 1979, p. 85.
[22] K.W. Hall, in: H.F. Barry, P.C.H. Mitchell (Eds.), Proceedings of the 4th Climax International Conference on the Chemistry and Uses of Molybdenum, Climax Molybdenum Golden, Colorado, 1982, p. 224.
[23] T. Ono, M. Anpo, Y. Kubokawa, J. Phys. Chem. 90 (1986) 4780.
[24] E.C. DeCanio, J.C. Edwards, T.R. Scalzo, D.A. Storm, J.W. Bruno, J. Catal. 132 (1991) 498.
[25] O.H. Han, C.Y. Lin, G.L. Haller, Catal. Lett. 14 (1992) 1.
[26] L.J. Lakshmi, P.K. Rao, V.M. Mastikhin, A.V. Nosov, J. Phys. Chem. 97 (1993) 11373.
[27] H. Kraus, R. Prins, A.P.M. Kentgens, J. Phys. Chem. 100 (1996) 16336.
[28] H. Kraus, R. Prins, J. Catal. 164 (1996) 251.
[29] H. Kraus, R. Prins, J. Catal. 170 (1997) 20.
[30] R. Iwamoto, C. Fernandez, J.P. Amoureux, J. Grimblot, J. Phys. Chem. B 102 (1998) 4342.
[31] R. Iwamoto, J. Grimblot, Stud. Surf. Sci. Catal. 127 (1999) 169.
[32] H. Ikeda, S. Morita, F. Katsuhisa, Nippon Ketjen Co. Ltd., PCT Int. Appl., WO 0209870 A2, 2002.

[33] L. Qu, R. Prins, J. Catal. 207 (2002) 286.
[34] L. Qu, R. Prins, J. Catal. 210 (2002) 183.
[35] E.R.H. Van Eck, R. Janssen, W.E.J.R. Maas, W.S. Veeman, Chem. Phys. Lett. 174 (1990) 428.
[36] H.W. Zandbergen, P.J. Kooyman, A.D. van Langeveld, in: Electron Microscopy, Proceedings ICEM 14, Cancun, Mexico (31 August–4 September, 1998), Symposium W, Vol. II, 1998, pp. 491–492.
[37] V.M. Mastikhin, I.L. Mudrakovsky, A.V. Nosov, Prog. Nucl. Magn. Reson. Spectrosc. 23 (1991) 259.
[38] E.C. DeCanio, J.C. Edwards, J.W. Bruno, J. Catal. 148 (1994) 76.
[39] H. Kraus, R. Prins, J. Catal. 164 (1996) 260.
[40] M. Hunger, Catal. Rev.-Sci. Eng. 39 (1997) 345.
[41] C.A. Fyfe, K.T. Muellar, H. Grondey, K.C. Woon-Moon, J. Phys. Chem. 97 (1993) 13484.
[42] G. Engelhardt, D. Michel, High-Resolution Solid-State NMR of Silicates and Zeolites, Wiley, New York, 1987.
[43] M. McMillan, J.S. Brinen, J.D. Carruthers, G.L. Haller, Colloids Surf. 38 (1989) 133.
[44] C. Dorémieux-Morin, C. Martin, J.-M. Brégeault, J. Fraissard, Appl. Catal. 77 (1991) 149.
[45] M. Hunger, J. Karger, H. Pfeifer, J. Caro, B. Zibrowius, M. Buelow, R. Mostowicz, J. Chem. Soc. Faraday Trans. 83 (1987) 3459.
[46] S. Axon, J. Klinowski, Appl. Catal. A 81 (1992) 27.
[47] W. Zhang, X. Han, X. Liu, X. Bao, Micropor. Mesopor. Mater. 50 (2001) 13.
[48] P. Arnoldy, J.C.M. de Jonge, J.A. Moulijn, J. Phys. Chem. 89 (1985) 4517.
[49] J. Brito, J. Laine, K.C. Pratt, J. Mater. Sci. 24 (1989) 245.
[50] J.A. Marzari, S. Rajagopal, R. Miranda, J. Catal. 156 (1995) 255.
[51] N.K. Nag, D. Fraenkel, J.A. Moulijn, B.C. Gates, J. Catal. 66 (1980) 162.
[52] B. Scheffer, P. Arnoldy, J.A. Moulijn, J. Catal. 112 (1988) 516.
[53] M. Daage, R.R. Chianelli, J. Catal. 149 (1994) 414.